

Controlled Confinement of Half-metallic 2D Electron Gas in BaTiO₃/Ba₂FeReO₆/BaTiO₃ Heterostructures: A First-principles Study

Santu Baidya^{1,*}, Umesh V. Waghmare¹, Arun Paramakanti^{2,3}, Tanusri Saha-Dasgupta^{4,†}

¹ *Jawaharlal Nehru Centre for Advanced Scientific Research, Jakkur, Bangalore 560064, India.*

² *Department of Physics, University of Toronto, Toronto, Ontario, Canada M5S 1A7.*

³ *Canadian Institute for Advanced Research, Toronto, Ontario, M5G 1Z8, Canada.*

⁴ *Department of Condensed Matter Physics and Materials Science, S. N. Bose National Centre for Basic Sciences, Kolkata 700 098, India.*

(Dated: October 26, 2015)

Using density functional theory calculations, we establish that the half-metallicity of bulk Ba₂FeReO₆ survives down to 1 nm thickness in BaTiO₃/Ba₂FeReO₆/BaTiO₃ heterostructures grown along the (001) and (111) directions. The confinement of the two-dimensional (2D) electron gas in this quantum well structure arises from the suppressed hybridization between Re/Fe *d* states and unoccupied Ti *d* states, and it is further strengthened by polar fields for the (111) direction. This mechanism, distinct from the polar catastrophe, leads to an order of magnitude stronger confinement of the 2D electron gas than that at the LaAlO₃/SrTiO₃ interface. We further show low-energy bands of (111) heterostructure display nontrivial topological character. Our work opens up the possibility of realizing ultra-thin spintronic devices.

PACS numbers: 71.20.Be, 71.15.Mb, 71.20.-b

A fundamental limit on device miniaturization is set by the size at which the material properties change qualitatively. This technologically important issue, has been studied for ferroelectrics, both, theoretically [1] and experimentally,[2] yielding a critical thickness of $\approx 12\text{\AA}$. [2] For spintronic devices, it is similarly important to explore how thin one can make half-metals (HMs), i.e., materials which conduct in one spin channel and insulate in another. It is of great technological interest if such device can further be made operative at high temperature.

In this Letter, we use first-principles density functional theory (DFT) to address this issue considering quantum wells of a double perovskite (DP) [3, 4] embedded in a wide band gap insulating oxide. In a heterostructure quantum well geometry, the electrons of the DP may be confined to 2D if potential energy mismatch can be created between the transition metal (TM) ions in the DP and in the insulating oxide, as in case of ultra-thin metallic layers of SrTi_{0.8}Nb_{0.2}O₃ embedded in insulating SrTiO₃ [5] or the (001) interface of SrTiO₃ with SrRuO₃. [6] This mechanism is different from polar catastrophe driven confinement of two dimensional electron gas, as found in well studied case of [100] interface of LaAlO₃ (LAO) and SrTiO₃ (STO), [7, 8] or recently studied interfaces and quantum well structures formed with GdTiO₃ (GTO) or SmTiO₃ (SmTO) and STO. [9, 10]

In particular, we focus on quantum wells formed by embedding the DP Ba₂FeReO₆ (BFRO), in the band insulator BaTiO₃ (BTO). The choice of BFRO is motivated by the fact that the bulk material is reported to be a half-metallic ferromagnet at room temperature, with $T_c \approx 304\text{K}$. [11] BTO is well-known to be a ferroelectric. However, we found that the ferroelectricity has little effect on the half-metallic properties of the embedded BFRO quantum well. Thus, we only present results here for

the cubic paraelectric phase of BTO. The comparison of structure and electronic properties considering the polar BTO surface in its ferroelectric phase is given in the supplementary material (SM). This choice of materials also ensures good lattice matching; the cubic lattice constants of BFRO and BTO being 4.025\AA and 4.009\AA , respectively. Finally, the synthesis of La_{0.7}Ca_{0.3}MnO₃ in contact with [001] surface of BaTiO₃ has been reported in the literature, [12] giving us confidence in realization of our proposed system. While oxide superlattices studied so far are grown along (001) direction, there has been recent progress on growth along the (111) direction, [13–15] propelled, in part, by theoretical predictions of exotic topological phases. [16–18] In particular, epitaxial growth of NdNiO₃ film on (111) direction has been achieved on a variety of substrate which includes LSAT, NdGaO₃ and LaAlO₃. [19] We therefore consider two growth directions, (111) and (001). BFRO has a nominal oxidation state of 5+ for Re and 3+ for Fe in BFRO, as shown by x-ray magnetic circular dichroism (XMCD) experiments, [11] while Ti in BTO has a nominal oxidation state 4+. This features nonpolar interfaces with a cubic symmetry for (001) heterostructure [cf. Fig 1(b,d)], and two polar interfaces, one of *n*-type and another of *p*-type, with a hexagonal symmetry [cf. Fig. 1(a,c)] for (111) heterostructure.

The 2D confinement in the BTO/BFRO/BTO quantum well structures studied here provides significant improvement over that in LAO/STO in terms of, (i) 2D confinement length being an order of magnitude smaller (ii) complete spin-polarization of the 2D electron gas (2DEG) (iii) polarity control of the 2DEG, suggestive of magnetoelectric coupling, and (iv) realization of ultra-thin half metals with topological bands. We note here even the most recent report of 2DEG at the surface of STO [20] is

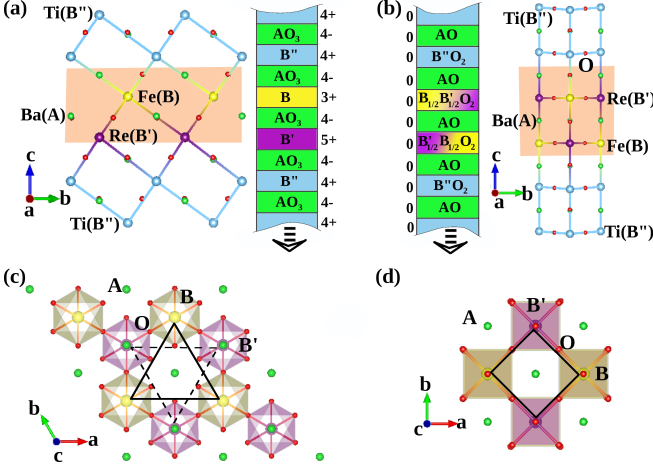


FIG. 1: (Color online) Geometry of BTO/BFRO/BTO heterostructures with c -axis oriented along the growth directions, (111) [panels (a), (c)] and (001) [panels (b), (d)]. Layer-wise nominal charges for the two heterostructures are shown in panels (a) and (b). The inplane honeycomb lattice with two triangular sublattices on different layers in case of (111) heterostructure and the inplane square lattice in case of (001) heterostructure are marked in panels (c) and (d), respectively.

found to be much less confined compared to that achieved in present study.

We use DFT calculations, within the generalized gradient approximation (GGA)[21] for the exchange-correlation functional, to study the electronic structure of bulk BFRO as well as the heterostructures. Our calculations are carried out using two choices of basis sets: (a) plane wave based pseudopotential method as implemented in the Vienna An-initio Simulation Package (VASP),[22] and (b) muffin tin orbital (MTO) based linear muffin tin orbital (LMTO)[23] and N-th order MTO (NMTO) method.[24] The calculations include spin-orbit coupling (SOC), which is important for Re 5d states. Details can be found in the supplementary material (SM).[25]

Bulk $\text{Ba}_2\text{FeReO}_6$ contains rocksalt arrangement of Fe and Re which are connected via O along all three crystallographic directions.[11] The quantum well structures are simulated by considering a supercell of cubic BaTiO_3 along desired crystallographic direction, (111) or (001), and replacing Ti cations by Fe and Re cations in two adjacent middle layers along c -direction of supercell. The inplane lattice constants of the supercells are fixed to that of the BaTiO_3 , which for (111) growth direction is $\sqrt{2/3}a_0$ and for (001) growth direction is $\sqrt{2}a_0$, a_0 being the cubic lattice constant of BTO. We completely relax the lattice parameter along the growth direction as well as all the atomic positions. In the buckled honeycomb lattice geometry for the (111) growth direction, this introduces trigonal distortion in BO_6 octahedra, signaled by the deviation of $\angle\text{O-B-O}$ from 90° . The optimized (111)

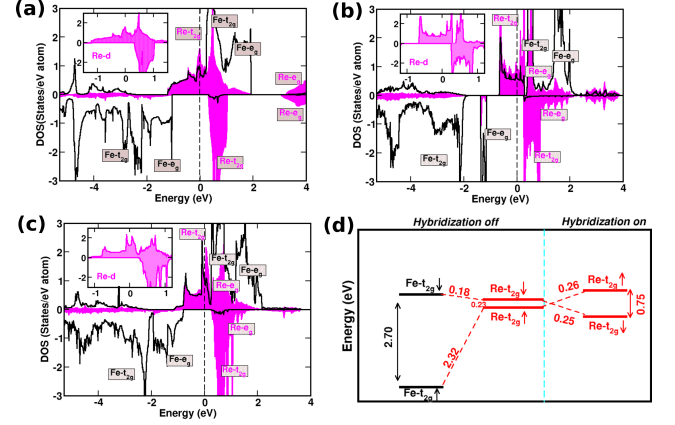


FIG. 2: (Color online) Density of states, projected onto Fe d (solid line) and Re d states (shaded area), in bulk BFRO [panel (a)], and in heterostructures along (111) [panel (b)] and (001) [panel (c)]. The zero of the energy is set at E_F . Panel insets show the zoomed DOS close to E_F . Panel (d) depicts the energy levels of Fe t_{2g} and Re t_{2g} in absence of the Fe-Re hybridization, and the renormalized Re t_{2g} energy positions after hybridization with Fe t_{2g} states. See text for details.

heterostructure shows this deviation to be 0.5° and 2.5° for ReO_6 and FeO_6 octahedra respectively. For the (001) heterostructure, the FeO_6 and ReO_6 octahedra upon optimization are found to be slightly elongated and contracted along the c -axis, respectively.

The GGA density of states (DOS), projected onto Fe d and Re d states in bulk BFRO as well as (111) and (001) heterostructures are shown in Fig. 2. The d states of Fe and Re are spin split as well as split by crystal field into nearly degenerate sets of t_{2g} 's and e_g 's. Considering the bulk DOS, Fe d states are found to be completely filled in the spin-down channel, separated by a gap of ≈ 1.2 eV from the empty Re t_{2g} states. In the spin-up channel, the Re t_{2g} states strongly hybridized with Fe t_{2g} states cross the Fermi level (E_F). This makes the system half-metallic with finite density of states at E_F in spin-up channel and zero in the spin-down channel, in agreement with literature.[11, 26] Remarkably, we find this continues to be the case even for (111) and (001) heterostructures with minimum thicknesses possible for BFRO in (111) and (001) directions. The inclusion of SOC is found to preserve the half-metallic character for both bulk BFRO and the heterostructures.[27] The large onsite energy difference between Ti^{4+} states and that of Fe/Re d states, makes the hybridization between the bilayer and the matrix of BTO negligibly small; the electronic structure close to E_F is thus dominated by Fe and Re d states. The bandwidths of the states are however significantly narrower than in bulk BFRO, especially in case of (111) heterostructure. Interestingly, we find the Re t_{2g} -Fe t_{2g} dominated states close to E_F in heterostructures show signature of 1D features characterized by van Hove singularities (see insets in Figs. 2(b) and 2(c)),

TABLE I: The spin (orbital) magnetic moment in μ_B , calculated within GGA+SO approximation, at Fe and Re sites for bulk $\text{Ba}_2\text{FeReO}_6$, and (111) and (001) bilayers of $\text{Ba}_2\text{FeReO}_6$.

	Bulk	(111)	(001)
Ions	Spin (Orbital)	Spin (Orbital)	Spin (Orbital)
Re	0.78 (-0.13)	0.79 (-0.13)	0.73 (-0.14)
Fe	-3.73 (-0.09)	-3.68 (-0.08)	-3.71 (-0.09)

signaling dimensional reduction.

The electronic structure of BFRO appears similar to the highly discussed DP $\text{Sr}_2\text{FeMoO}_6$ [28] or Cr-based 3d-5d DPs,[29] suggesting that the hybridization-driven mechanism is operative for magnetism of BFRO, as in these other cases. In order to probe this further, we calculate the energy level positions of Fe t_{2g} 's and Re t_{2g} 's in bulk BFRO employing NMTO downfolding. In absence of hybridization between Fe t_{2g} 's and Re t_{2g} 's, obtained considering a Fe t_{2g} - Re t_{2g} active basis set, the energy levels of Re t_{2g} states appear in between the spin split Fe t_{2g} states [cf Fig. 2(d)]. Considering the Re t_{2g} only active basis set, which takes into account hybridization effect between Fe t_{2g} and Re t_{2g} states, it is found that the hybridization between Fe t_{2g} and Re t_{2g} states, pushes up (down) the renormalized Re t_{2g} up (down) spin states. This leads to a renormalized spin splitting at Re site directed oppositely to that of Fe, enforcing ferromagnetic alignment of Fe spins, induced solely by hybridization effect. This hybridization driven mechanism works whenever Re atoms have appreciable number of Fe neighbors connected through sharing O, as in case of (111) and (001) heterostructures.

The calculated spin and orbital magnetic moments at Re and Fe sites are listed in Table I. For bulk BFRO, these are in reasonable agreement with that predicted from neutron powder diffraction.[11] We note here the moment at Re ion is somewhat different between our calculation and that reported by Wu.[26] This deviation results from use of different basis set, different exchange-correlation functional and most importantly neglect of spin-orbit coupling in the calculation of Wu.[26] The moments are found to be rather similar between the bulk BFRO and the heterostructures, reconfirming that the basic electronic structure of BFRO remains intact in the heterostructure, except for the reduction in dimensionality. To check the effect of correlation beyond GGA, we carried out GGA+U+SOC calculations, with a choice of $U_{Fe} = 4$ eV, $U_{Re} = 2$ eV and $J_H = 0.8$ eV. The qualitative picture is found to survive, specially the half-metallic character, with larger moments on Fe and Re due to slight reduction in bandwidths. The spin(orbital) moments are found to be between -4.1 and $-4.2 \mu_B$ (-0.04 and $-0.06 \mu_B$) at Fe site and -1.1 and $-1.3 \mu_B$ (-0.10 and $-0.12 \mu_B$) at Re site.

To appreciate the effect of SOC in the band structure

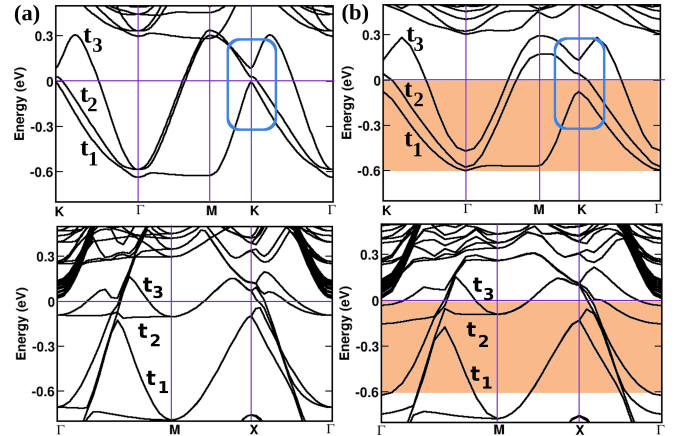


FIG. 3: (a) The GGA (left panels) and GGA+SO (right panels) band structures of (111) (top panels) and (001) (bottom panels) heterostructures plotted along the high symmetry directions. For (111) heterostructure, the chosen high symmetry directions are $K = (0.3333, 0.3333, 0)$, to $\Gamma = (0, 0, 0)$ to $M = (0.5, 0.0, 0)$ to K to Γ . For (001) heterostructure, the chosen high symmetry directions are Γ to $M = (0.5, 0.5, 0.0)$ to $X = (0.0, 0.5, 0.0)$ to Γ . Zero of the energy is set at respective E_F 's. Blue rectangular area highlights the band topology at high symmetry K point in (111) heterostructure.

in heterostructure geometry, which may have important bearing on the topological nature of the bands of the bilayer, we show in Fig. 3, the band structure of both the heterostructures computed within GGA+SO, in comparison to that of GGA. In case of (111) heterostructure, three isolated Re t_{2g} bands cross E_F having admixture from Fe. The band structure of (001) heterostructure, on the other hand, is far more complicated with both Fe d and Ti d states crossing the manifold of Re t_{2g} bands. While the effect of SOC is found to be not very significant for (001) case, in case of (111) heterostructure the effect is found to be significant. We find the (111) GGA band structure at the K-point shows near degeneracy of the three bands. This follows the small trigonal distortion at Re site, leading to only tiny trigonal splitting. Switching on the SOC coupling pushes the t_1 and t_3 bands away from each other at K point, though the whole band structure remains as metal with highly dispersive bands crossing E_F . Since the (111) bilayer band structure consists of isolated bands near E_F a Chern number of each of these bands can be defined. The three isolated, spin-polarized, and dominantly Re bands near the Fermi level can be modeled using a tight-binding model for t_{2g} orbitals on the 2D triangular lattice formed by Re atoms on the (111) face. Computing the Berry curvature of the resulting tight-binding bands (see SM), we find that, in increasing order of energy at the Γ -point, the bands have Chern numbers $-2, 2, 0$. Thus, the combination of SOC and low dimensionality, drives topological half-metallic bands with large Chern number. Though the t_1 and t_2 bands are found to have nontrivial Chern numbers, the

solution turns out to be metallic rather than insulating. This happens as the crystal field splitting is not large enough, needed to push the t_1 and t_2 bands sufficiently far from each other. The (111) bilayer thus can be a quantum anomalous Hall insulator, if t_1 and t_2 bands can be prevented from spanning a common energy window. This may be possible through strain engineering, which will be a topic of future study.

The presence of van Hove singularities in the low energy electronic structure of (111) and (001) bilayers strongly suggests reduction of dimensionality of the half-metallic conducting electrons compared to bulk BFRO. From the plot of the charge density, as shown in Figs 4(a) and 4(b) for (111) heterostructure, and Figs 4(c) and 4(d) for (001) heterostructure, we find the conduction charges to be entirely localized in the bilayer of BFRO, with little contribution in BTO block. The conducting charge confined in the BFRO bilayer are distributed within the Re and Fe sites, connected via oxygens forming a highly mobile and spin-polarized 2DEG. In order to have quantitative estimates of the confinement, the layer averaged charge density is computed and plotted as a function of position along the growth direction. The results are shown in Fig 4(e). For nonpolar (001) interfaces, the concentration profile is symmetric, with a spread of about 14Å. Changing the growth direction to (111) with creation of polar interfaces makes the concentration profile asymmetric with a drastic reduction in spread to only about 7Å, which is of the order of unit cell thickness of BFRO. We contrast this with the confinement of the 2DEG formed at the (001) LAO/STO interface, keeping in mind that the origin of confinement is different in the two cases. The infrared ellipsometry data [30] shows the vertical concentration profile of the electrons at the LAO/STO interface has a strong asymmetric shape with a initial decay over 2 nm and a pronounced tail that extends to ~ 11 nm, an order of magnitude larger than in BTO/BFRO/BTO.

We compute effective masses corresponding to the three t_{2g} bands at Γ point showing parabolic or near parabolic dispersion. The bands falling in this region (shaded) are marked in Fig. 3. Effective mass tensor $m_{ij}^{-1} = \frac{1}{\hbar} \frac{\partial^2 E}{\partial k_i \partial k_j}$ is computed using finite difference method in unit of rest mass m_0 . The inplane and out-of-plane effective masses for (111) and (001) heterostructures are tabulated in Table II, which further brings out the highly confined 2D mobile character of the carriers.

To conclude, our DFT study establishes that BTO/BFRO/BTO heterostructure geometry generates spin polarized 2D electron gas at the interface confined solely to the BFRO bilayer, which retains the half-metallic character of bulk BFRO. The confinement is driven by suppression of hybridization, a mechanism distinct from the polar catastrophe driven confinement of the 2DEG realized at the (001) LAO/STO or GTO/STO

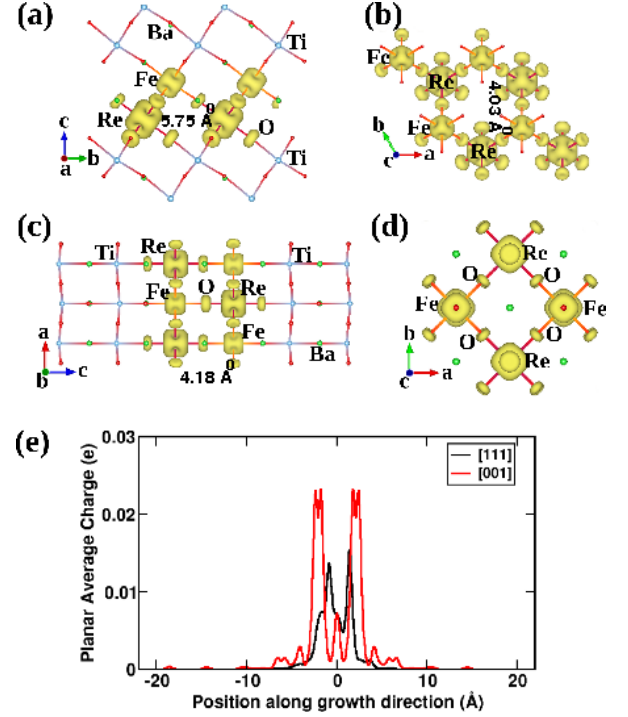


FIG. 4: Out-of-plane and inplane projection of the conducting charge density in (111) [panels (a) and (b), respectively] and (001) heterostructure geometries [panels (c) and (d), respectively]. The isosurface values are chosen as $0.023e^-/\text{\AA}^3$. The charge densities are calculated from contributions within an energy window $[E_F - 0.5eV, E_F]$. Various atomic distances have been marked. Panel (e): Planar averaged conducting charge density versus distance along the growth direction for (111) and (001) heterostructures. The distances are measured from the centre of the unit cell, which is at the mid point of the bilayer.

TABLE II: Inplane and out-of-plane effective masses of the conducting bands for (111) and (001) heterostructures, calculated at Γ point.

	Band#	m_{\parallel}^{eff}	m_{\perp}^{eff}		Band#	m_{\parallel}^{eff}	m_{\perp}^{eff}
(111)	3.	$1.2 m_0$	$22 m_0$	(001)	3.	$2.3 m_0$	$73 m_0$
	2.	$0.8 m_0$	$840 m_0$		2.	$1.0 m_0$	$73 m_0$
	1.	$3.6 m_0$	$61 m_0$		1.	$7.8 m_0$	$5.6 m_0$

or SmTO/STO interfaces. For the (111) orientation, the confinement of the 2DEG is greatly aided by polar fields at the interface, leading to confinement width of the order of unit cell thickness and an order magnitude smaller than that reported for LAO/STO. This highly confined 2D electron gas which is half-metallic in nature, with a moment $\approx 3.0 \mu_B/\text{unit cell}$, should be promising for applications in ultra-thin spintronic devices. Bulk BFRO has a room temperature magnetic transition temperature of 304 K and a significant magnetocrystalline anisotropy $\approx 1\text{-}2$ meV.[31] The proposed half-metallic quantum well structure is thus expected to be operative at a reasonably

high temperature and stable against magnetic spiral instabilities due to Rashba SOC. We further find that the interface bands of (111) structure have topological character, with the potential to realize the quantum anomalous Hall effect. With insulating nature of the BTO layers, this heterostructure also naturally permits top or bottom gating to control the transport in the 2DEG, making it suitable for hybrid spintronic and electronic devices. Our computational study provides strong motivation for experimental investigations of half-metallic 2DEGs in oxide quantum wells.

S.B. and T.S.D thank Department of Science and Technology, India for the support through Thematic Unit of Excellence. AP was supported by NSERC (Canada).

* Presently at University of Duisburg-Essen, Duisburg.

† Email: t.sahadasgupta@gmail.com

-
- [1] N.A. Spaldin, *Science*, **304**, 1606 (2004).
 - [2] D. D. Fong *et al.* *Science*, **304**, 1650 (2004).
 - [3] M. Anderson, K. Greenwood, G. Taylor and K. Poepelmeier, *Prog. Solid State Chem.*, **22**, 197 (1993).
 - [4] T. Saha-Dasgupta, *J Supercond Nov Magn* **26** 1991 (2013); DOI 10.1007/s10948-012-1920-7
 - [5] H Ohta *et al.*, *Nat. Mater.* **6**, 129 (2007).
 - [6] M. Verissimo-Alves, P. Garcia-Fernandez, D. I. Bilc, Ph. Ghosez and J. Junquera. *Phys. Rev. Lett.* **108**, 107003 (2012).
 - [7] A. Ohtomo and H. Y. Hwang, *Nature (London)* **427**, 423 (2004).
 - [8] A. Ohtomo, D. A. Muller, J. L. Grazul, and H. Y. Hwang, *Nature (London)* **419**, 378 (2002).
 - [9] Pouya Moetafeg, Tyler A. Cain, Daniel G. Ouellette, Jack Y. Zhang, Dmitri O. Klenov, Anderson Janotti, Chris G. Van de Walle, Siddharth Rajan, S. James Allen, and Susanne Stemmer, *App. Phys. Lett.* **99**, 232116 (2011).
 - [10] Jack Y. Zhang, Clayton A. Jackson, Ru Chen, Santosh Raghavan, Pouya Moetafeg, Leon Balents and Susanne Stemmer, *Phys. Rev. B* **89**, 075140 (2014).
 - [11] C. Azimonte, J. C. Cezar, E. Granado, Q. Huang, J. W. Lynn, J. C. P. Campoy, J. Gopalakrishnan and K. Ramesha, *Phys. Rev. Lett.* **98**, 017204 (2007).
 - [12] Y. P. Lee *et al.* *Phys. Rev. B* **73** 224413 (2006).
 - [13] M. Gibert, P. Zubko, R. Scherwitzl, J. Iniguez, and J. M. Triscone, *Nature Materials* **11**, 195 (2012).
 - [14] B. Gray, H.-N. Lee, J. Liu, J. Chakhalian, and J. W. Freeland, *Appl. Phys. Lett.* **97**, 013105 (2010).
 - [15] D. Hirai, J. Matsuno, H. Takagi, *APL Materials* **3**, 041508 (2015).
 - [16] D. Xiao, W. Zhu, Y. Ran, N. Nagaosa and S. Okamoto, *Nature Commun* **2** 596 (2011).
 - [17] X. Hu, A. Rüegg, and G. A. Fiete, *Phys. Rev. B* **86**, 235141 (2012).
 - [18] A. M. Cook and A. Paramekanti, *Phys. Rev. Lett.* **113**, 077203 (2014).
 - [19] S. Catalano *et al.*, *APL Materials* **3**, 062506 (2015).
 - [20] Z. Wang *et al.* *PNAS* **111**, 3933 (2014).
 - [21] J. P. Perdew, K. Burke, and M. Ernzerhof, *Phys. Rev. Lett.* **77**, 3865 (1996).
 - [22] G. Kresse *et al.*, *Phys. Rev. B* **54**, 11169 (1996).
 - [23] O. K. Andersen and O. Jepsen, *Phys. Rev. Lett.* **53**, 2571 (1984).
 - [24] O. K. Andersen and T. Saha-Dasgupta, *Phys. Rev. B* **62**, R16219 (2000).
 - [25] The supplementary material contains the details of the computation as well as details on the calculation of Chern numbers based on tight-binding models.
 - [26] H. Wu, *Phys. Rev. B* **64** 125126 (2001).
 - [27] The spin-orbit coupling being included in the calculation as a second variational approach, the assignment of up and down channels refers to S_z states derives, from a projection onto non-eigenstate basis functions. The spin splitting being large, the mixing driven by spin raising and lowering operator is estimated to be small.
 - [28] D.D. Sarma *et al.*, *Phys. Rev. Lett.* **85**, 2549 (2000).
 - [29] Hena Das, Prabuddha Sanyal, T. Saha-Dasgupta, and D. D. Sarma, *Phys. Rev. B* **83**, 104418 (2011).
 - [30] A. Dubroka *et al.*, *Phys. Rev. Lett* **104** 156807 (2010).
 - [31] K. W. Plumb, A. M. Cook, J. P. Clancy, A. I. Kolesnikov, B. C. Jeon, T. W. Noh, A. Paramekanti, Young-June Kim, *Phys. Rev. B* **87**, 184412 (2013).